Korean J. Chem. Eng., 19(1), 1-10 (2002)
FEATURED REVIEW

Surface Science Studies of Ziegler-Natta Olefin Polymerization System: Correlations between Polymerization Kinetics, Polymer Structures, and Active Site Structures on Model Catalysts

Seong Han Kim*, Craig R. Tewell and Gabor A. Somorjai†

Department of Chemistry, University of California at Berkeley and Materials Science Division, Lawrence Berkeley National Laboratory, Berkeley, CA 94720, USA

Abstract–The surface composition and structure of model Ziegler-Natta catalysts, polymerizing α-olefins to produce polyolefins, have been studied using modern surface science techniques and compared with their polymerization behaviors. Two types of thin films - $TiCl_x/MgCl_2$ and $TiCl_y$/Au - were fabricated on an inert gold substrate, using chemical vapor deposition methods, to model the high-yield catalysts of $MgCl_2$-supported $TiCl_4$ and $TiCl_3$-based catalysts, respectively. The model catalysts could be activated by exposure to triethylaluminum ($AlEt_3$) vapor. Once activated, both catalysts were active for polymerization of ethylene and propylene in the absence of excess $AlEt_3$ during polymerization. The model catalysts had polymerization activities comparable to the high-surface-area industrial catalysts. Though both catalysts were terminated with chlorine at the surface, each catalyst assumed different surface structures. The $TiCl_x/MgCl_2$ film surface was composed of two structures: the (001) basal plane of these halide crystallites and a non-basal plane structure. The $TiCl_y$/Au film surface assumed only the non-basal plane structure. These structural differences resulted in different tacticity of the polypropylene produced with these catalysts. The $TiCl_x/MgCl_2$ catalyst produced both atactic and isotactic polypropylene, while the $TiCl_y$/Au catalyst without the $MgCl_2$ support produced exclusively isotactic polypropylene. The titanium oxidation state distribution did not have a critical role in determining the tacticity of the polypropylene.

Key words: Ziegler-Natta, Polymerization Catalyst, Active Sites, Stereochemistry

INTRODUCTION

The surface structure of polymerization sites of the titanium chloride catalysts are one of the most important - but least understood - parameters in heterogeneous Ziegler-Natta polymerization systems producing poly-α-olefins because they determine the stereochemistry of the polymerization process as well as the polymerization rate [Boor, 1979; Keii, 1972; Kissin, 1985; Fink et al., 1994; Barbè et al., 1986; Dusseault and Hsu, 1993; Xie et al., 1994; Soga and Shiono, 1997]. For this reason, a great number of experimental studies have been carried out to understand and control the surface properties of the Ziegler-Natta catalysts. Most of these conventional studies reported in literature focused on bulk analyses of the catalysts produced by different preparation methods and product analyses of the polymers produced by these catalysts [Boor, 1979; Keii, 1972; Kissin, 1985; Fink et al., 1994; Barbè et al., 1986; Dusseault and Hsu, 1993; Xie et al., 1994; Soga and Shiono, 1997]. However, these analyses could not provide an unambiguous description of the nature of active sites on the catalyst surface. The molecular-level understanding of the heterogeneous Zieglar-Natta catalysts could be possible only through direct characterization of the surface properties of the catalyst at various stages of polymerization using state-of-the-art surface science techniques.

†To whom correspondence should be addressed.
E-mail: shkim@engr.psu.edu
*Present address: Assistant Professor, Department of Chemical Engineering, The Pennsylvania State University, University Park, PA 16803, USA

Surface science studies of the Ziegler-Natta polymerization system can be done for model systems fabricated in ultra-high vacuum (UHV) conditions [Magni and Somorjai, 1995a, b, c, 1996a, b, 1997, 1998; Kim and Somorjai, 2000a, b, c, 2001; Kim et al., 2000a, b, 2001]. Thin films of magnesium chloride, titanium chloride, and their mixtures were produced, as model catalysts for the Ziegler-Natta polymerization, via modified chemical vapor deposition methods. These model catalysts can be analyzed using x-ray photoelectron spectroscopy (XPS), temperature programmed desorption (TPD), ion scattering spectroscopy (ISS), low energy electron diffraction (LEED), Auger electron spectroscopy (AES), and UV Raman spectroscopy for characterization of surface compositions and surface structures. Polymerization kinetics of the model catalysts can be studied by laser reflection interferometry (LRI). These studies showed that the thin-film model catalysts have polymerization activities comparable to high-surface-area catalysts in ethylene and propylene polymerization. The produced polymers can be analyzed with IR and Raman spectroscopy, solvent fractionation, and atomic force microscopy (AFM) to determine stereochemistry of the polymerization process. These surface science approaches in our laboratory made it possible to find correlations between the surface properties of the catalyst and its polymerization behaviors.

This review describes recent progress that resulted from our surface science studies on model Ziegler-Natta polymerization catalysts: (1) the surface structure of the $MgCl_2$ substrate, (2) the chlorine termination of the catalyst surface, (3) the importance of the unsaturated Mg sites at the $MgCl_2$ surface for $TiCl_4$ adsorption, (4) the adsorption site distribution on the catalyst surface, (5) the Ti

oxidation state distribution before and after the $AlEt_3$ activation, (6) propylene polymerization with the catalyst containing mostly Ti^{3+} and Ti^{4+}, (7) polymer morphology during the polymerization and its possible role in the catalyst deactivation, and (8) the correlation between the surface site distribution and the stereoregularity in propylene polymerization. We also developed new techniques: halide film deposition methods in UHV to fabricate model catalysts, mesitylene thermal desorption to study the catalytically active adsorption sites, laser reflection interferometry to measure polymerization kinetics on a flat catalyst sample and UV Raman spectroscopy that can be applied to microporous catalysts [Tewell et al., submitted].

SURFACE SCIENCE APPROACHES

Many surface science techniques utilize electrons or ions as a surface probe [Somorjai, 1994; Woodruff and Delchar, 1994]. Because of their high cross-sections in interactions with the condensed phase, electrons and ions interact mostly with species in the first few layers at the solid surface. Thus, any information they carry originates from the surface region. Direct applications of these surface-sensitive techniques to non-conductive materials, however, are limited due to surface charging. This limitation could be overcome by preparing the catalyst in thin film form on a conducting substrate [Gunter et al., 1997; Rainer and Goodman, 1998]. Thermal evaporation and modified chemical vapor deposition methods were used to produce a $MgCl_2$ multilayer film, a titanium chloride layer chemisorbed on a $MgCl_2$ multilayer film ($TiCl_x/MgCl_2$), and a titanium chloride multilayer film ($TiCl_x$/Au) on a polycrystalline gold substrate. These chloride thin films could be fabricated reproducibly in UHV and studied in situ without any significant charging problems (see Section III).

Spectroscopic techniques used for surface characterization were LEED, AES, ISS, and XPS. Details about these techniques can be found elsewhere [Somorjai, 1994; Woodruff and Delchar, 1994]. LEED, a two-dimensional version of x-ray diffraction, was used to obtain information on the structure of the $MgCl_2$ film. AES gave information on the near-surface chemical composition and film growth mechanisms of the model catalyst film. The chemical composition of the outermost surface was determined by ISS. One drawback of the LEED, AES, and ISS techniques was that the incident electron and ions irradiation could damage the halide film surfaces. Information on the chemical environment of the atoms in the near-surface region, such as elemental oxidation states, was obtained with XPS. The photoelectron spectrum in the binding energy region of 5-40 eV was used for identification of the polymer in the surface region because each polymer has a characteristic valence band spectrum.

TPD provided information on thermal decomposition and sublimation of the model catalyst film. The film was heated at a linear rate, and the desorbing species were detected with a quadrupole mass spectrometer (QMS). In TPD of the mesitylene-covered catalyst surface, the heat of mesitylene desorption provided information about the surface structure of the model catalyst film [Kim and Somorjai, 2000a, 2001; Kim et al., 2001].

The polymerization rate on the model catalyst was measured with LRI. This technique is based on the refractive index difference between the polymer and the catalyst [Zuiker et al., 1995]. The polymer film thickness was obtained by solving the Fresnels equations for light reflection, and the polymer amount was calculated by multiplying the polymer thickness with the catalyst surface area and the polymer density. The morphology and mechanical properties of the polymer, produced with the model catalysts, were studied with AFM.

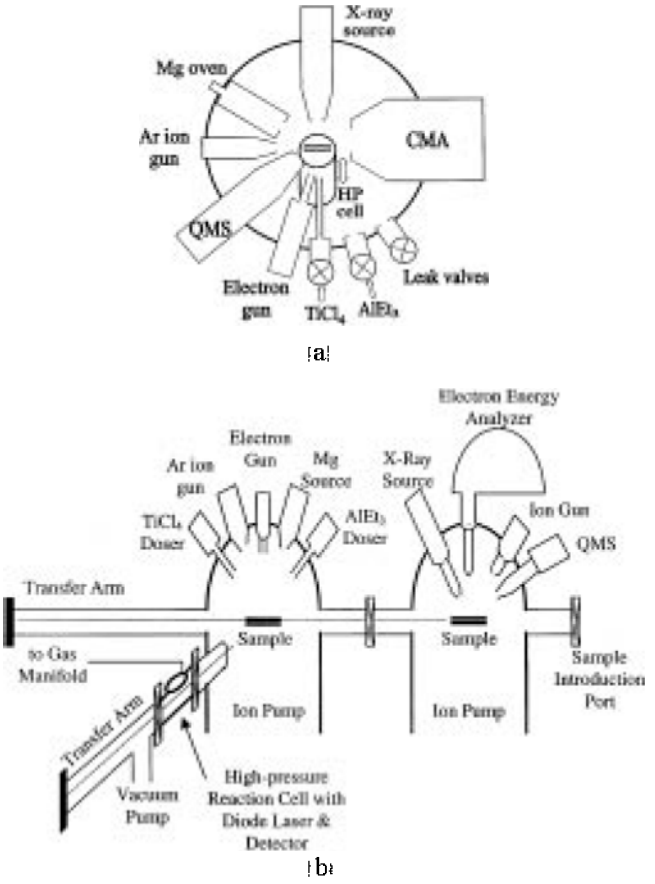

Fig. 1. Schematic views of UHV chambers used in surface science studies of model Ziegler-Natta polymerization system.

In this study, two UHV chambers equipped with high-pressure reaction cells were used in the surface science studies of the model Ziegler-Natta catalyst system. Fig. 1 shows their schematic views. The base pressures of both chambers were maintained at about $1 \cdot 10^{-9}$ Torr. One chamber (Fig. 1a) was equipped with a sputter ion gun for surface cleaning, an x-ray source and a double-pass cylindrical mirror analyzer (CMA) with a co-axial electron gun for XPS and AES, a QMS for residual gas analysis and TPD. A commercially available sample manipulator provided three-dimensional translation and 360° rotation of the sample. This chamber also had three leak valves for gas exposure, a Knudsen cell for Mg dosing, an electron flood gun for model catalyst preparation, and an internal high-pressure reaction cell (HP) for in-situ polymerization. The other chamber (Fig. 1b) consisted of a preparation chamber, an analysis chamber, and a high-pressure reaction cell. The preparation chamber was equipped with an Ar ion sputter gun, a Mg source (Knudsen cell), an electron gun, and leak valves. The analysis chamber housed a PHI 5400 ESCA system for XPS and ISS. The reaction cell was equipped with a temperature-controlled diode laser (λ=

675 nm) and a photodetector for *in situ* LRI measurements of polymer film growth. The model catalyst sample under study was transferred from one section of the apparatus to the others without exposure to air. Further details of these chambers were given elsewhere [Kim and Somorjai, 2000a, b; Kim et al., 2000b].

UV Raman spectroscopy was utilized to study $MgCl_2$ and ethanol (EtOH) complexes that are used for preparation of microporous supports for Ziegler-Natta polymerization catalysts. Characterization of these supports is important because it is known that fabrication conditions markedly affect the polymerization process, the molecular weight distribution, the isotacticity of polypropylene, and the mechanical properties of polymers. The use of UV as an excitation source can avoid fluorescence interference from the catalyst that often overwhelms the Raman signal of the species of interest in the visible spectrum. More details can be found in Ref. 31.

FABRICATION AND CHARACTERIZATION OF MODEL CATALYSTS

1. Model Supports

1-1. $MgCl_2$ Thin Film in UHV

$MgCl_2$ films were grown by thermal evaporation of $MgCl_2$ on gold. AES and XPS analyses showed that the film grows via a layer-by-layer mechanism [Magni and Somorjai, 1995a, b]. ISS experiments revealed that the film is Cl terminated at the surface. LEED studies of multilayer $MgCl_2$ films, deposited in similar conditions on Pd (111), Pd (100) Pt (111), Pt (100)-hex and Rh (111), indicated that these films expose the Cl-terminated (001) basal plane of the α-$MgCl_2$ bulk structure at the solid-vacuum interface [Fairbrother et al., 1997, 1998; Roberts et al., 1998].

$TiCl_4$ did not chemisorb on these films by simple exposure to the $TiCl_4$ vapor at 300 K in UHV [Magni and Somorjai, 1995a]. The growth of titanium chloride layers was achieved by Mg-induced or electron-induced $TiCl_4$ deposition as described in Section III-2a.

1-2. $MgCl_2$-EtOH Complexes

The samples were synthesized by addition of pure EtOH to crystalline α-$MgCl_2$ in precise stoichiometric amounts, folloed by heating to 180 °C and slow cooling to room temperature [Tewell et al., submitted]. This entire procedure was performed in an inert, dry atmosphere.

Fig. 2 shows the Raman spectra of a series $MgCl_2$:$EtOH_x$ adducts with x=0.5, 2, and 6. The A_{1g} mode of $MgCl_2$ at 240 cm^{-1} is observed for x<2. This mode is no longer present for the x=2 adduct, indicating a complete loss of the D_{3d} symmetry of $MgCl_2$. For x>3.5, a peak at 683 cm^{-1} is observed which is not found in liquid ethanol. Based on the structure of $MgCl_2$:$EtOH_6$ determined from x-ray diffraction [Valle et al., 1989], the 683 cm^{-1} peak was assigned to the A_{1g} mode of Mg-O octahedra. In addition, the position of the O-H stretch shifts from 3,480 to 3,230 m^{-1} as x increases from 0 to 6 relative to $MgCl_2$ (data not shown). This O-H peak shift resulted from hydrogen bond- ing of the OH groups with chlorine atoms and could be utilized to monitor the $MgCl_2$:EtOH molar ratio during sample preparation.

2. Model Catalysts

In case of high-surface-area catalysts, $MgCl_2$ powders are mechanically ground for $TiCl_4$ fixation. But, mechanical grinding is not suitable in UHV conditions. We developed two chemical vapor deposition schemes for fabrication of model catalysts in UHV: reac-

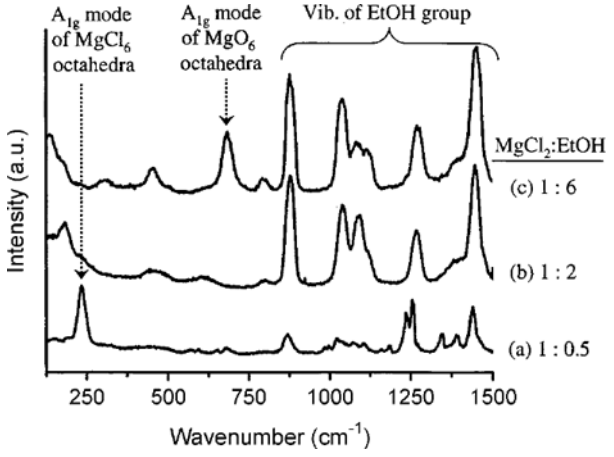

Fig. 2. UV Raman spectra of powered $MgCl_2$:$EtOH_x$ adducts with x=0.5, 2, and 6. The peaks above 800 cm^{-1} originate from vibrations of EtOH. In spectrum (a), the peaks circa 1,250-1,400 cm^{-1} are due to air, not EtOH.

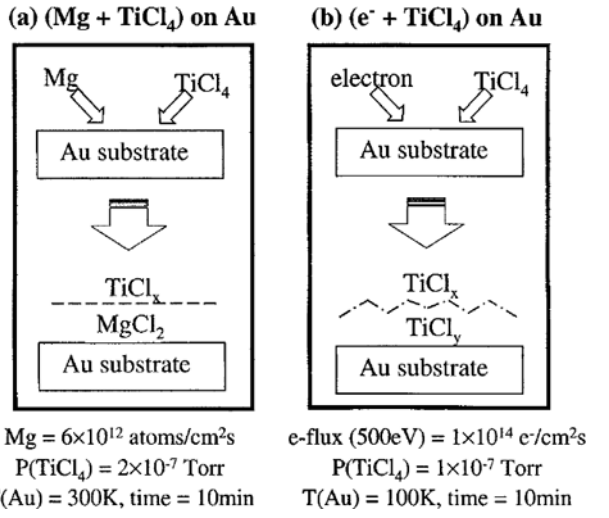

Fig. 3. Deposition of model catalysts via (a) reactions of Mg and $TiCl_4$ and (b) dissociation of $TiCl_4$ by electrons.

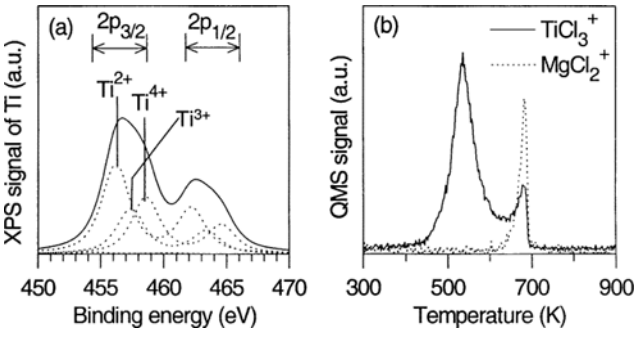

Fig. 4. (a) XPS and (b) TPD of a $TiCl_x$/$MgCl_2$ film fabricated by co-deposition of Mg and $TiCl_4$. Heating rate=2 K/sec. Deposition conditions: T_{Mg}=600 K; P($TiCl_4$)=2×10^-7 Torr; time =5 min.

tions of Mg with $TiCl_4$ (Fig. 3a) and dissociation of $TiCl_4$ with electrons (Fig. 3b). The former produced a thin film modeling $MgCl_2$-supported $TiCl_4$ and the latter produced one modeling $TiCl_3$-based catalysts. Each case is described in detail below.

2-1. $TiCl_x/MgCl_2$ Film as a Model System for the $MgCl_2$-Supported $TiCl_4$ Catalysts

Reduction-oxidation reactions of metallic Mg and $TiCl_4$, deposited simultaneously from the vapor phase onto a Au substrate, produced the model catalyst film of $TiCl_x/MgCl_2$ (Fig. 3a) [Magni and Somorjai, 1998; Kim and Somorjai, 2000b]. The low solubility of $TiCl_x$ in $MgCl_2$ led to the formation of a $TiCl_x$ monolayer on top of $MgCl_2$ multilayers characteristic of the supported catalysts. XPS revealed that the Ti oxidation states had a distribution of 4+, 3+, and 2+ (Fig. 4a). The $TiCl_4$/Mg flux ratio during the deposition controlled the oxidation state distribution and surface coverage of $TiCl_x$ species of the deposited film. The surface $TiCl_x$ species desorb as $TiCl_4$ upon heating the co-deposited film at temperatures higher than 430 K (Fig. 4b).

The reaction of a pre-deposited Mg film with the $TiCl_4$ vapor also produced the $TiCl_x/MgCl_2$ model catalyst [Kim and Somorjai, 2000b]. In this case, the Mg atoms in the underlayer were not converted to $MgCl_2$ due to a kinetic barrier for chlorine diffusion. Upon heating this sequentially deposited film, the chlorine ions near the surface region diffused and reacted with metallic Mg atoms in underlayers to complete the redox reaction.

The $MgCl_2$ film surface could be activated for $TiCl_4$ fixation by irradiation of high-flux electrons of 1 keV [Magni and Somorjai, 1996a]. ISS showed that under-coordinated Mg atoms were left on the film surface after the preferential desorption of Cl atoms by electron irradiation. The formation of under-coordinated Mg atoms at the $MgCl_2$ film surface allowed for the chemisorption of $TiCl_4$ near room temperature.

2-2. $TiCl_y$ Multilayer Film as a Model System for the $TiCl_3$-based Catalysts

The multilayer $TiCl_y$ film was prepared by electron-induced deposition of $TiCl_4$ on Au (Fig. 3b) [Magni and Somorjai, 1996a; Kim and Somorjai, submitted]. In this method, the substrate was irradiated by a high-energy electron beam (500-1,000 eV) during the $TiCl_4$ exposure. Upon collision with the substrate, the incident electrons produced scattered and secondary electrons that had higher cross sections for dissociation of $TiCl_4$. A faster growth rate and larger surface roughness of the film was achieved for deposition at a cryogenic temperature (100 K) compared to deposition at room temperature (300 K). The oxidation state distribution of titanium ions in the film could be controlled with deposition temperature, post-deposition electron irradiation, and annealing [Kim and Somorjai, submitted]. The low temperature deposition produced a film containing more Ti^{4+} species-chemisorbed $TiCl_4$- at the film surface (Fig. 5). The post-deposition elec- tron irradiation reduced the high oxidation-state Ti ions to lower oxidation states. Upon heating the $TiCl_y$/Au films, the surface Ti^{4+} species desorbed as $TiCl_4$ at the temperatures higher than 400 K. After annealing at 580 K, the film remained on Au showed mostly Ti^{2+} with a small amount of Ti^{4+} in XPS.

With the electron-induced $TiCl_4$ deposition method, a multilayer film of $TiCl_y$ could grow on top of the $MgCl_2$ film [Magni and Somorjai, 1996b]. The $TiCl_y/MgCl_2$ film grown at 300 K had the Ti oxidation state distribution similar to that of $TiCl_y$/Au grown at 300 K. Angle-resolved XPS analysis indicated that both $TiCl_y$ films consist of a monolayer of Ti^{4+} species on top of $TiCl_2$ layers.

SURFACE ADSORPTION SITES ON $TiCl_x/MgCl_2$ AND $TiCl_y$/Au MODEL CATALYSTS

1. $TiCl_x/MgCl_2$ Films and $MgCl_2$ Films

The adsorption site distribution on the model Ziegler-Natta catalyst surfaces was measured with TPD of mesitylene as a probe molecule [Kim and Somorjai, 2000a; Kim et al., 2001]. Though this method could not distinguish the metal composition (Ti vs. Mg) and oxidation state (Ti^{4+} vs. Ti^{2+}) due to chlorine termination of the catalyst surface, it could differentiate various adsorption sites which have different structures of surface chlorine [Kim et al., 2001].

Comparison of weakly bound mesitylene desorption profiles for $TiCl_x/MgCl_2$ and $MgCl_2$ identified the presence of two types of surface adsorption site structures on the model catalyst film (Fig. 6): a site producing mesitylene desorption peak at ~200 K and a site producing mesitylene desorption peak at ~250 K). Annealing at 640 K did not change the distribution of these two sites.

Since the exact surface structure of the active site was not known, the mesitylene TPD data were interpreted on basis of crystallo-

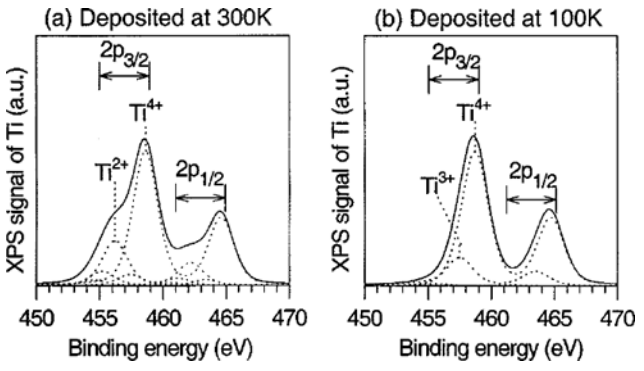

Fig. 5. XPS of $TiCl_y$/Au films fabricated by 500 eV electron-induced deposition at (a) 300 K and (b) 100 K. Electron flux= 1.5×10^{14} electrons/cm^{2}sec. P($TiCl_4$)=1×10^{-7} Torr. Deposition time=(a) 30 min and (b) 15 min.

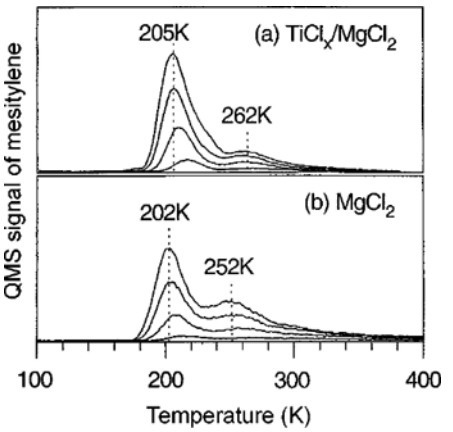

Fig. 6. Mesitylene TPD of (a) $TiCl_x/MgCl_2$ and (b) $MgCl_2$ films deposited at 300 K. Mesitylene exposure=0.2, 0.6, 1.0, 1.4 L (1 L=1×10^{-6} Torr·s).

graphic data [Allegra, 1995], surface structure [Fairbrother et al., 1998], surface compositions [Magni and Somorjai, 1995a, b], the shape of micro-crystals [Rodriguez et al., 1966; Guttman and Guillet, 1968], and thermodynamics [Lin and Catlow, 1993; Colbourn et al., 1994] of the titanium chloride and magnesium chloride films or crystals obtained by other techniques. X-ray diffraction (XRD) found that these halide crystals have a layered structure, each layer consisting of two monoatomic layers of chlorine ions octahedrally coordinated to intercalating metal ions [Allegra, 1995]. The low-energy electron diffraction (LEED) study of a $MgCl_2$ film, deposited by thermal evaporation in UHV, showed that the film grows layer-by-layer and the film surface was composed of small domains of the (001) basal plane, the most stable crystallographic plane [Fairbrother et al., 1998; Lin and Catlow, 1993; Colbourn et al., 1994]. The He^+ ion scattering spectroscopy (ISS) studies of the model Ziegler-Natta catalyst films found that the surfaces of these films are terminated with chlorine ions and no metal ions are exposed to vacuum [Magni and Somorjai, 1995b, c, 1996b]. The SEM pictures described that the $TiCl_3$ micro-crystallites, produced by a sublimation-recrystallization method, possess a very thin, hexagonal platelet shape [Rodriguez et al., 1966; Guttman and Guillet, 1968]. The hexagonal symmetry of the $TiCl_3$ unit cell suggested that the platelet surface assume the (001) basal plane structure and only one crystallographic plane is dominant for the sides of the crystals. This plane is most likely to be the (100) plane, the second most stable plane of the crystal [Lin and Catlow, 1993; Colbourn et al., 1994].

Assuming this structural information is applicable to the model catalyst films, we could attribute the dominant mesitylene desorption peak at ~200 K for $TiCl_x/MgCl_2$ to a basal plane structure where the chlorine ions at the outermost layer are close packed and the metal ions under the chlorine layer are coordinated to six chlorine atoms [Kim et al., 2001]. In this circumstance, the high-temperature desorption peak at 246 K could tentatively be attributed to a non-basal plane where the surface chlorine ions are not close packed and the metal ions under the chlorine layer are under-coordinated [Kim et al., 2001]. The possible candidates would be the crystallographic dislocations on the basal plane or other crystallographic planes at the boundaries of the (001) basal plane (see refs. 3, 6, 7, or 37 for crystallographic models).

The metal composition (Ti versus Mg) could not be differentiated due to the chlorine termination of the catalyst surface [Magni and Somorjai, 1995b; Kim et al., 2001]. Other crystallographic planes such as (100) and (110) could not be distinguished with mesitylene TPD. This could be attributed to the higher surface energies of these planes compared to the (001) basal plane [Lin and Catlow, 1993]. If these planes were exposed at the surface, they would reconstruct or react with $TiCl_4$ and/or residual gas (HCl) to lower surface energy.

The mesitylene TPD technique also found diffusion of the bulk chlorine atoms to the surface to lower the film surface energy [Kim et al., 2001]. When the chlorine-deficient defect sites were generated to a concentration higher than thermodynamic equilibrium by electron irradiation or metallic Mg dose, the bulk chlorine atoms diffused to the surface and reacted with the defect sites even at temperatures lower than room temperature. At room temperature, the diffusion process was remarkably fast.

2. $TiCl_y$/Au Films

The surface structure of $TiCl_y$/Au differed from those of $TiCl_x$/$MgCl_2$ and $MgCl_2$, as revealed by mesitylene TPD (Fig. 7). The $TiCl_y$/Au film deposited at 100 K was almost completely covered with chemisorbed $TiCl_4$ from which mesitylene desorbed at ~220 K. After removal of the chemisorbed species by annealing at 580 K, the $TiCl_y$/Au film showed mostly the coordinatively unsaturated sites (mesitylene desorption=~250 K). The absence of the mesitylene desorption at ~200 K for $TiCl_y$ catalyst implied that the $TiCl_y$ film surface was dominantly composed of the non-basal plane structure containing under-coordinated metal-ions [Kim and Somorjai, 2001, submitted]. The electron bombardment during the deposition process appeared to be responsible for the structural deviation of $TiCl_y$/Au [Kim et al., 2001, submitted]. Electrons of high kinetic energy induced chlorine desorption from the surface. The $TiCl_y$/Au film deposited at 300 K show a mesitylene desorption peak at ~260 K and no peak at ~200 K [Kim and Somorjai, in press]. These results indicated that the $TiCl_y$/Au film deposited by electron irradiation has only the coordinatively unsaturated sites at the surface.

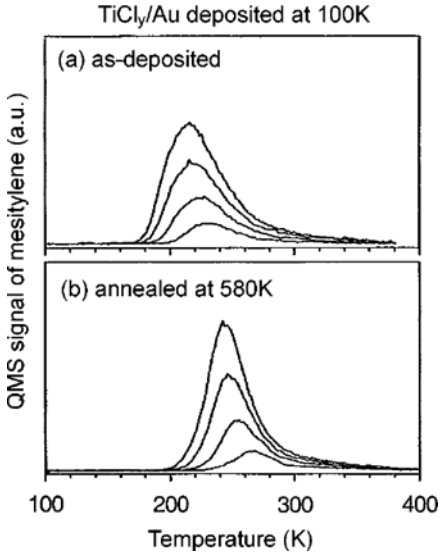

Fig. 7. Mesitylene TPD of a multilayer film of $TiCl_y$/Au deposited at 100 K. Mesitylene exposure=0.2, 0.6, 1.0, 1.4 L.

ACTIVATION OF THE MODEL CATALYSTS WITH THE $AlEt_3$ CO-CATALYST

The reduction and alkylation of the $TiCl_4$ chemisorbed at the model catalyst surface have been monitored by XPS [Magni and Somorjai, 1997; Kim et al., 2001; Kim and Somorjai, 2001]. Large exposures of $AlEt_3$ (10^2-10^6 L) were required to reduce and alkylate the $TiCl_x/MgCl_2$ and $TiCl_y$/Au films at 300 K. In XPS, the decrease of the Ti^{4+} peak was accompanied by the increase of Ti^{2+} peak (Fig. 8). The Ti^{3+} species was not observed as a main product of the $AlEt_3$ activation in XPS. The absence of the Al peak in XPS suggested that the Al containing species were not chemically bonded to the catalyst surface and desorbed into vacuum.

After the catalyst activation by reaction with the $AlEt_3$ co-catalyst, the mesitylene desorption profiles were shifted to lower temperatures (Fig. 9) [Kim et al., 2001; Kim and Somorjai, 2001]. The basal plane sites showed a decrease of 4-5 K in the peak desorption temperature of mesitylene, while the coordinatively unsaturated

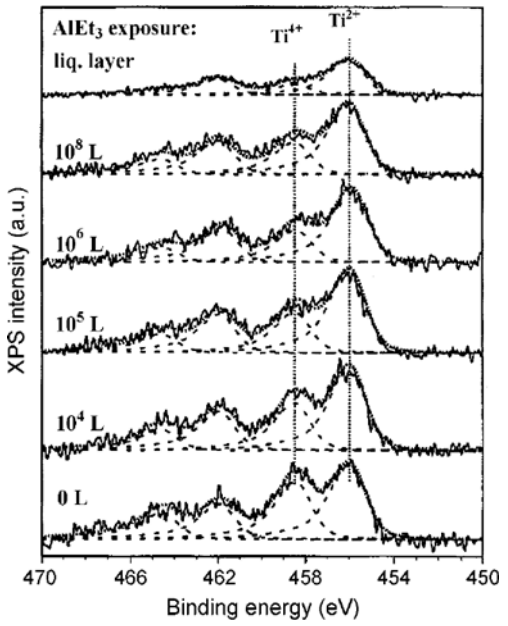

Fig. 8. Ti 2p region of the XPS spectra of a $TiCl_x/MgCl_2$ film as a function of $AlEt_3$ exposure at 300 K (ref. 13).

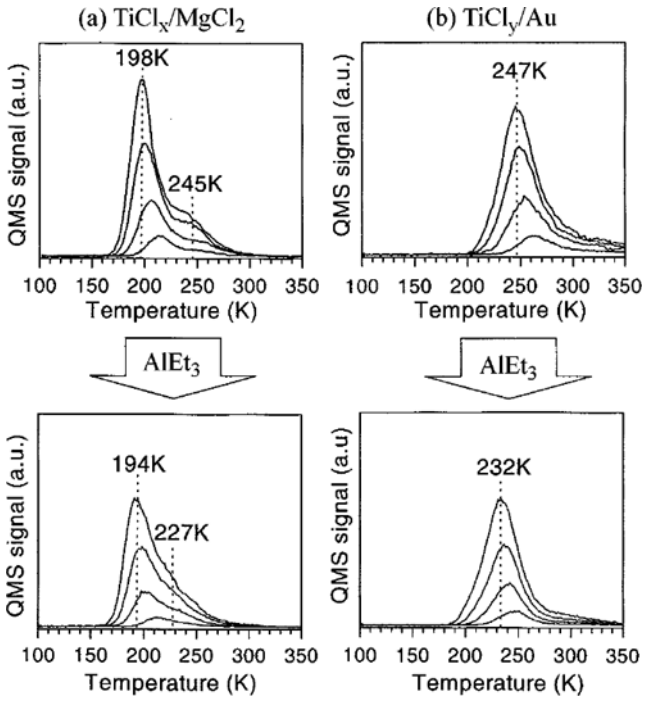

Fig. 9. Mesitylene TPD profiles of (a) $TiCl_x/MgCl_2$ and (b) $TiCl_y$/Au catalysts before and after $AlEt_3$ activation. The catalyst activation process was exposure to 1 Torr of $AlEt_3$ vapor for 1 min. Mesitylene exposure=0.2, 0.6, 1.0, 1.4 L (1 L=1×10^{-6} Torr·s).

sites showed a larger decrease of ~15 K. If one accepts the existing model for catalyst alkylation [Arlman and Cossee, 1964; Rodriguez et al., 1966], the changes in the mesitylene desorption temperature could be explained as below. For the basal plane sites, the alkylation by $AlEt_3$ would replace one Cl anion with a C_2H_5 group [Arlman and Cossee, 1964; Rodriguez et al., 1966]. This would induce only a minor change in the mesitylene-surface interactions (only 2 K shift in the peak desorption temperature). For the non-basal plane sites of $TiCl_x/MgCl_2$ and $TiCl_y$, the alkylation by $AlEt_3$ would occur by addition of one C_2H_5 group to the under-coordinated metal ions [Arlman and Cossee, 1964; Rodriguez et al., 1966]. So, the alkylated non-basal plane sties would assume a more close packed structure that would have weaker interactions with mesitylene, causing a larger decrease (about 15 K) in the mesitylene desorption temperature. This was consistent with the effects of the aluminum alkyl reaction on the adsorption isotherm of allene, a molecule poisoning the catalytic activity, reported by Petts and Waugh [Petts and Waugh, 1982]. The heat of allene adsorption showed a larger decrease for the high-temperature sites after the activation of a high-surface-area catalyst with trimethyl aluminum. Both catalysts retained their original distribution of the surface adsorption sites.

Once activated with $AlEt_3$, the model catalysts were active for both ethylene and propylene polymerization, regardless of the presence of the gas-phase $AlEt_3$ in the reaction cell [Magni and Somorjai, 1995c; Kim et al., 2000b; Kim and Somorjai, 2000c].

POLYMERIZATION WITH MODEL CATALYSTS

1. Polymerization Kinetics for $TiCl_x/MgCl_2$

The polymerization rates for the model catalysts of a surface area of ~1 cm^2 were measured with LRI (Fig. 10). The changes of periodicity of the interference fringes indicated a slow decrease of the growth rate with increasing polymer film thickness [Kim et al., 2000b]. The deactivation of polymerization rate appeared to be due to the monomer diffusion that was controlled by the thickness and morphology of the growing polymer film. The decrease in the interference peak intensity was caused by roughness of the polymer film surface, inhomogeneity in the film density, or porosity of the film. The morphology of the polymer film changed in a complex way as a function of polymerization time.

The initial polymerization rates of the model catalysts were 2-4 · 10^{-6} g-C_2H_4/cm^2-cat·sec for propylene and 5-9 · 10^{-7} g-C_2H_4/cm^2-cat·sec for ethylene. These polymerization rates corresponded to nominal turnover frequencies of 3-6 · 10^{14} C_2H_5 molecules per cm^2

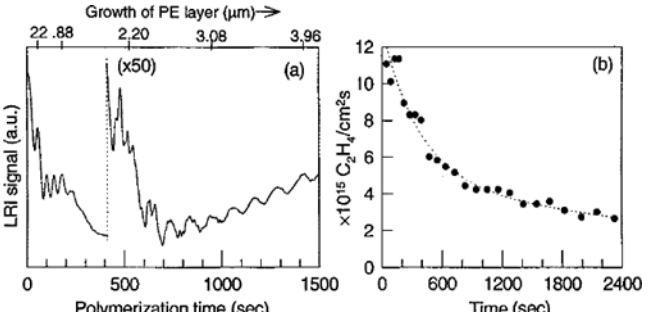

Fig. 10. (a) LRI signal and (b) polymerization rate as a function of time during the ethylene polymerization on a $TiCl_x/MgCl_2$ model catalyst. Polymerization was performed with 900 Torr of ethylene in the presence of the $AlEt_3$ (5 Torr) in the gas phase. The reactor temperature was kept at 340 K. In (b), the density of the polyethylene film produced was assumed to be 0.96.

of catalyst per second and 1-1.8 · 10^{16} C_2H_4 molecules per cm^2 of catalyst per second, respectively. The propylene polymerization rate was about 30 times slower than the ethylene polymerization rate on the same catalyst.

Converted with a typical surface area of industrial catalysts (~50 m^2/g), the polymerization activity of the model catalyst corresponded to ~75 g-PP/g-cat·hr·atm and ~1,400 g-PE/g-cat·hr·atm, respectively. Industrial catalysts produce about 100-500 g-PP/g-cat·hr·atm and 2,000~10,000 g-PE/g-cat·hr·atm [Kissin, 1985; Barbè et al., 1986]. While the precise values were difficult to compare due to the differences in catalyst preparation and polymerization conditions, we concluded that the model catalyst displays a polymerization activity of the same order of magnitude as its industrial counterparts.

2. Titanium Oxidation States of the Polymerization Sites

Successful polymerization of propylene with the model catalysts containing mostly Ti^{2+} and Ti^{4+} were quite interesting because there has been a consensus that only the catalysts containing Ti^{3+} can polymerize propylene [Soga et al., 1981a, b; Kashiwa and Yoshitake, 1984]. The titanium oxidation distribution observed in this study was consistent with the XPS [Hasebe et al., 1997] and electrochemical data [Kashiwa and Yoshitake, 1984] obtained for high-surface area catalysts; but not consistent with the data determined from a combination of wet redox titration and electron spin resonance (ESR) [Fuhrmann and Herrmann, 1994; Brant and Speca, 1987; Chien and Wu, 1985; Chien and Hu, 1989; Chien et al., 1989]. The latter approaches have reported that the Ti^{3+} species are a major product of the catalyst activation by $AlEt_3$. Based on these ESR studies and other kinetic studies, it has long been suggested and believed that only the Ti^{3+} species, formed by the $AlEt_3$ activation, can polymerize propylene [Barbè et al., 1986]. However, it should be noted that the Ti^{2+} and Ti^{4+} ions are not ESR active and more than 80% of total Ti^{3+} ions in the Ziegler-Natta catalysts are ESR silent due to interactions with the adjacent Ti^{3+} ions [Fuhrmann and Herrmann, 1994; Brant and Speca, 1987]. *In situ* measurements of *both* XPS and ESR for the same catalyst sample would provide answer to this discrepancy.

3. Location of the Active Sites During Polymerization

The location of the active sites can be determined from the XPS analysis of the polymer film produced by sequential polymerization of different monomers [Kim and Somorjai, 2000c]. If the active sites remain at the interface of the polymer and the catalyst phase and the polymer grows over the active sites [Mckenna et al., 1995; Hamba et al., 1997; Shariati et al., 1999], the first-polymerized layer would be located on top of the second-polymerized layer. If the active sites are separated from the catalyst surface and migrate to the interface of the polymer and the gas phase and the polymer grows under the active sites [Böhm, 1978; Spitz et al., 1984], the first-polymerized layer would be found under the second-polymerized layer. If the catalyst phase undergoes significant fragmentation as polymerization occurs [Gutman and Guillet, 1970; Kakugo et al., 1989; Santa Maria et al., 1993; Noristi et al., 1994], the surface composition of the sequentially polymerized film would have both polymer components depending on the degree of the catalyst fragmentation.

Fig. 11 shows the valence-band XPS of the sequentially polymerized film (230 nm-thick PP first then 780 nm-thick PE second) was compared with those of pure PP and PE films grown separately. The PE film had two C2s peaks at ~14 and 18.3 eV that corresponded to the antibonding and bonding orbitals of the carbon in the $-CH_2-$ backbone, respectively [Gross et al., 1994; Delhalle et al., 1993]. The PP film had an additional C2s peak at 16 eV of the carbon in the $-CH_3$ group. In the case of the sequentially polymerized film, the C2s spectrum showed three peaks characteristic of the PP film and no contribution from the PE film. This result indicated that the first-polymerized PP layer was at the film surface and the second-polymerized PE layer was under the PP layer. Therefore, the active sites for polymerization remain at the polymer/substrate interface. Fig. 12 illustrates the polymerization process where the active sites are located at the bottom of the growing polymer layer and the monomer molecules are transported through the polymer layer to the active sites.

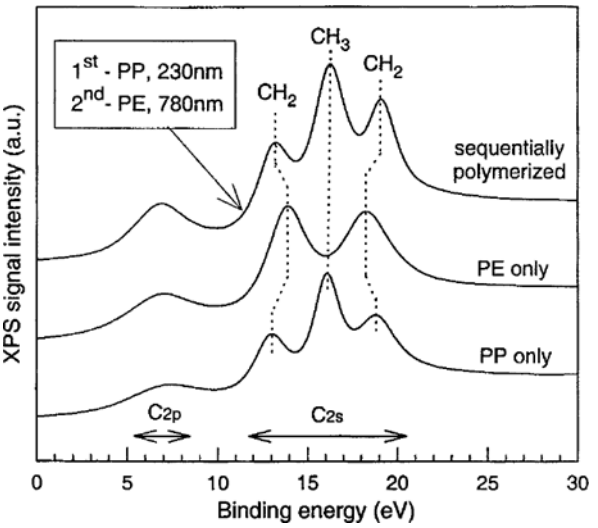

Fig. 11. Valence band XPS spectrum of the sequentially grown polymer film (230 nm-thick PP first; then 780 nm-thick PE second) and comparison with those of pure polyethylene and polypropylene films grown separately. The peaks at ~13 eV and ~19 eV result from the C2s antibonding and bonding orbitals of $-CH_2-$ in the polymer backbone, respectively. The peak at 16 eV comes from the C2s orbital of the CH_3 group. The photoelectrons from the C2p orbitals appear at around 7 eV (Pass energy of XPS measurements=35.75 eV).

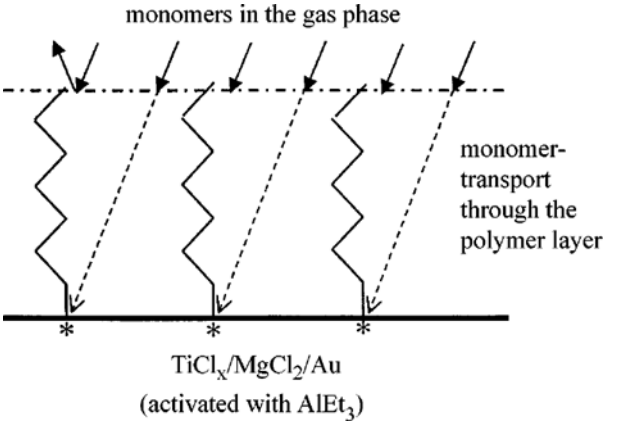

Fig. 12. Schematic illustration for polymer growth at the polymer/catalyst interface.

The aluminum-containing species, such as $AlEt_2Cl$ produced as results of the catalyst activation with $AlEt_3$, are not involved in polymerization the active sties located at the bottom of the polymer film. When the ethylene polymerization was carried out in the presence of excess $AlEt_3$ (5 Torr) in the gas phase, XPS detected small Al peaks only at the film/gas phase interface. When the PE film was peeled off from the substrate, no Al peaks were detected at the bottom of the PE film peeled off from the substrate after polymerization. This observation ruled out a bimetallic active site model [Keii et al., 1982; Kohara et al., 1979]. Furthermore, this result indicated that once the polymer film covers the catalyst surface, there is no additional effect of excess $AlEt_3$ on the polymerization kinetics of the active sites under the polymer film.

4. Correlation between Catalyst Surface Structure and Polypropylene Tacticity

Since the polymerization always occurred at the catalyst surface, the catalyst surface structure affected the stereochemistry of the polymerization process [Kim and Somorjai, 2001]. In order to mimic the $MgCl_2$-supported $TiCl_4$ and the $TiCl_3$-based systems, two types of titanium chloride model catalysts - with and without $MgCl_2$ support - were fabricated by co-deposition of Mg and $TiCl_4$ and electron-induced deposition of $TiCl_4$, respectively, as described in the previous sections. The comparison of the mesitylene desorption profiles of the $TiCl_x/MgCl_2$ and $TiCl_y/Au$ catalysts (Fig. 9) clearly showed that the surface structure of $TiCl_x/MgCl_2$ differed from that of $TiCl_y/Au$ [Kim et al., 2001]. In mesitylene TPD, both basal plane sites (198 K) and non-basal plane sites (245 K) were observed for the $TiCl_x/MgCl_2$ catalyst, while only non-basal plane sties (247 K) were seen for the $TiCl_y$ catalyst. There was no discernible peak at 200 K for the $TiCl_y/Au$ catalyst. The first-order desorption profile of mesitylene and its narrow peak width (fwhm=30~40 K), as shown in Fig. 12b, could suggest that the catalyst surface assume only one dominant structure.

The catalyst activation by reactions with the $AlEt_3$ co-catalyst shifted the mesitylene desorption profiles to lower temperatures, but it did not change their original distribution of the surface adsorption sites (Fig. 9) [Kim et al., 2001; Kim and Somorjai, 2001]. In XPS analysis, the oxidation state distributions of the activated surface species of these two catalysts appeared to be very close to each other [Kim et al., 2001; Kim and Somorjai, 2001].

Propylene polymerization was carried out with the two catalysts after mesitylene TPD and XPS analyses. The atactic and isotactic fractions of the PP films produced were separated into a 'hexane-soluble' fraction and a 'hexane-insoluble/octane-soluble' fraction, respectively [Hayashi et al., 1989; Busico et al., 1991; Paukkeri et al., 1993], and then analyzed with AFM. Figs. 13a and 13b show AFM images of atactic and isotactic fractions of PP, respectively, produced with $TiCl_x/MgCl_2$. At a low load (0.6 nN), both atactic and isotactic PP were imaged intact. However, at a high load (2 nN), the atactic PP pushed out from the scan region, while the isotactic PP was remained intact. This behavior was consistent with the material properties of atactic and isotactic PP, confirming the conformation of each extracted PP fraction [Gracias and Somorjai, 1998]. The isotactic PP was much harder than atactic PP [Lorenzo et al., 1989; Ogawa, 1992] so that it was able to sustain the pressure generated by the AFM tip at the high load condition (also see Fig. 13d).

In the case of the PP sample produced with the $TiCl_y$ catalyst,

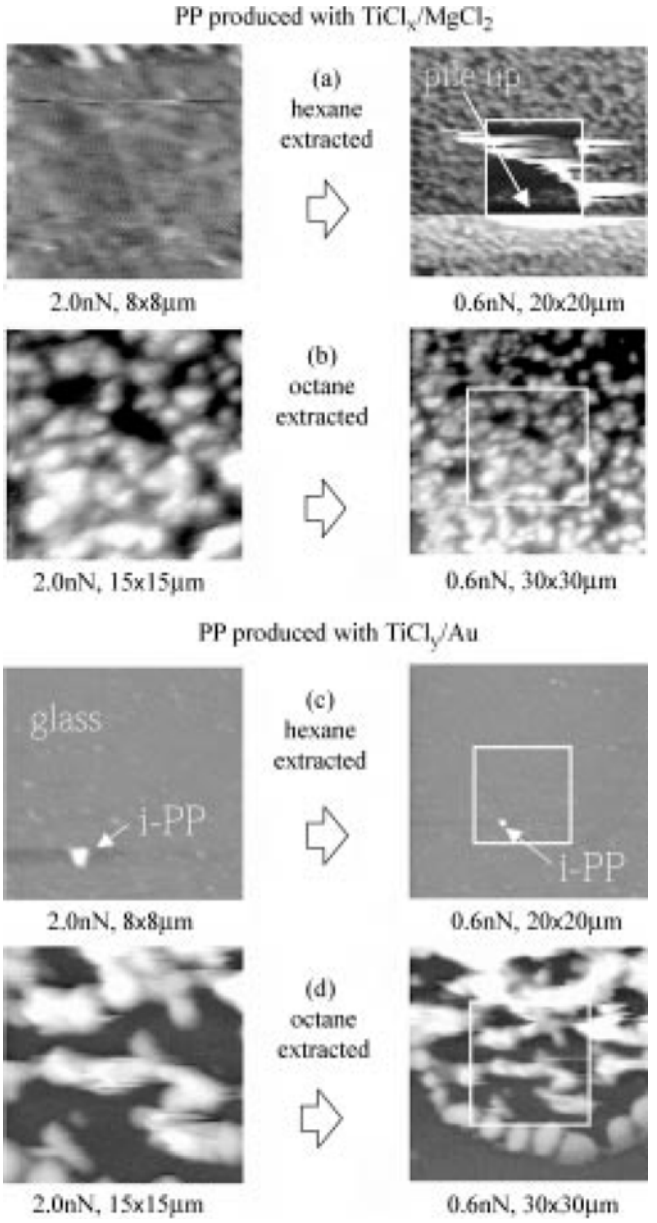

Fig. 13. AFM images of (a) hexane-soluble fraction and (b) hexane-insoluble/octane-soluble fraction of polypropylene produced with the $TiCl_x/MgCl_2$ catalyst and (c) hexane-soluble fraction and (d) hexane-insoluble/octane-soluble fraction of polypropylene produced with the $TiCl_y$ catalyst. The polymerization was carried out after activation of the catalysts with $AlEt_3$ followed by structural analysis with mesitylene TPD in UHV (Fig. 9) (Monomer pressure =900 Torr, reaction temperature=340 K).

Fig. 13c clearly shows the absence of the atactic fraction. A small particle in Fig. 13c was believed to be isotactic PP based on its hardness. Therefore, it could be concluded that the the $TiCl_x/MgCl_2$ model catalyst produces both atactic and isotactic polypropylene, while the $TiCl_y$ catalyst produces exclusively isotactic polypropylene. The ATR-IR analysis of the as-grown PP film supported this conclusion [Kim and Somorjai, 2001]. The production of PP with different tacticity from the $TiCl_x/MgCl_2$ and $TiCl_y/Au$ catalysts was consistent with a typical polymerization behavior of the industrial coun-

terparts of the Ziegler-Natta catalysts: in the absence of electron donors such as ethyl benzoate, the $MgCl_2$-supported $TiCl_4$ catalyst produces less isotactic polypropylene than the $TiCl_3$-based catalyst [Kissin, 1985, p. 295].

These data were probably the first experimental observation proving directly the correlation between the structures of the catalyst surfaces and the stereospecificity of propylene polymerization [Arlman and Cossee, 1964; Cossee, 1964; Arlman, 1964; Guerra et al., 1987; Venditto et al., 1991; Cavallo et al., 1998; Shiga et al., 1994, 1995; Puhakka et al., 1995, 1997; Boero et al., 1998, 1999, 2000]. The surface of the $TiCl_x/MgCl_2$ catalyst, producing both atactic and isotactic polypropylene, consisted of two types of adsorption site structures. In contrast, the $TiCl_y$ catalyst consisted predominantly of one adsorption site structure and produced exclusively isotactic propylene. The absence of the basal plane sites (Fig. 12b) and the absence of the atactic PP fraction (Fig. 13c) clearly suggested that the active sites of this structure are stereochemically nonspecific. The Ti oxidation state distribution did not seem to be an important factor in stereoregularity because their distribution at the catalyst surfaces were not significantly different form each other.

FUTURE PROSPECTS

Several fundamental problems still remain unsolved, such as the knowledge of the precise configuration of the active centers and the mechanisms involving the elementary polymerization steps. This information could be obtained with surface-sensitive vibrational spectroscopic techniques such as infrared-visible sum-frequency generation (SFG). The IR-Vis SFG technique is a second-order nonlinear optical spectroscopy capable of providing surface specific vibrational spectra in the range of 1,000-4,000 cm^{-1} under an atmosphere of background gases with excellent resolution and signal-to-noise ratio [Shen, 1989; Su et al., 1996, 1997; Zhang et al., 1997]. Therefore, the SFG measurements during the polymerization will provide structural information on the hydrocarbon intermediates during the monomer insertion reactions on the catalyst surface. The broad-band SFG, using a femtosecond laser, will be able to obtain the vibration spectrum of the surface intermediates in the initial polymerization stages with an excellent time resolution ($>10^{-12}$ sec).

The detailed structure of the non-basal plane sites is not determined yet. The mesitylene TPD was able to distinguish these sited from the basal plane sites. A simple crystallographic consideration could suggest many possible structures for this non-basal plane such as (100), (110), etc. The $MgCl_2$(100) surface has the Mg atoms coordinated to five chlorine atoms. The $MgCl_2$(110) surface has the Mg atoms coordinated to four chlorine atoms. However, these surfaces have high surface energies structures and undergo significant reconstruction processes [Lin and Catlow, 1993; Colbourn et al., 1994]. Structural imaging of the (100) and (110) planes of a $MgCl_2$ single crystal, using scanning tunneling microscopy, would provide more insight into the surface structure of the non-basal planes where isotactic polypropylene is produced.

From an industrial perspective, surface science techniques can provide a way to modify the surface of the current catalyst or to invent new synthetic routes to produce a single-site catalyst. For example, high-energy electron, photon or ion irradiation of the catalyst surface can generate a new adsorption site structure. Reactions of metallic titanium with $MgCl_2$ or alkyl halide are expected to produce a model catalyst film with a surface structure different than those prepared with the current synthetic methods. Reaction of titanium atoms with $TiCl_4$ would produce $TiCl_3$-nanoparticles that might have unique polymerization properties. Adsorption of appropriate molecules could be used to selectively poison the non-stereospecific polymerization sites on the supported catalysts. The mesitylene TPD technique appears to be a suitable method to monitor the changes on the treated surface.

ACKNOWLEDGEMENTS

This work was supported by the Director, Office of Energy Research, Office of Basic Energy Sciences, Materials Sciences Division, of the US Department of Energy under Contract No. DE-AC03-76SF00098. The authors also acknowledged support from MONTELL USA, Inc.

REFERENCES

Allegra, G., *Macromol. Symp.*, **89**, 163 (1995) and see references therein.
Arlman, E. J., *J. Catal.*, **3**, 89 (1964).
Arlman, E. and Cossee, P. J., *J. Catal.*, **3**, 99 (1964).
Barbè, P. C., Cecchin, G. and Noristi, L., *Adv. Polym. Sci.*, **81**, 1 (1986).
Boero, M., Parrinello, M. and Terakura, K., *J. Am. Chem. Soc.*, **120**, 2746 (1998).
Boero, M., Parrinello, M. and Terakura, K., *Surf. Sci.*, **438**, 1 (1999).
Boero, M., Parrinello, M., Huffer, S. and Terakura, K., *J. Am. Chem. Soc.*, **122**, 501 (2000).
Boor, Jr. J., "Ziegler-Natta Catalysis and Polymerization," Academic Press, New York (1979).
Brant, P. and Speca, A. N., *Macromolecules*, **20**, 2740 (1987).
Busico, V., Coradini, P., De Martino, L., Graziano, F. and Iadicicco, A., *Makromol. Chem.*, **192**, 49 (1991).
Böhm, L. L., *Polymer*, **19**, 545 (1978).
Cavallo, L., Guerra, G. and Corradini, P., *J. Am. Chem. Soc.*, **120**, 2428 (1998).
Chien, J. C. W. and Hu, Y., *J. Polym. Sci. A*, **27**, 897 (1989).
Chien, J. C. W. and Wu, J.-C., *J. Polym. Sci. Polym. Chem. Ed.*, **20**, 2461 (1982).
Chien, J. C. W., Weber, S. and Hu, Y., *J. Polym. Sci. A*, **27**, 1499 (1989).
Colbourn, E. A., Cox, P. A., Carruthers, B. and Jones, P. J. V., *J. Mater. Chem.*, **4**, 805 (1994).
Cossee, P. J., *J. Catal.*, **3**, 80 (1964).
Delhalle, J., Riga, J., Denis, J. P., Deleuze, M. and Dosiere, M., *Chem. Phys. Lett.*, **210**, 21 (1993).
Dusseault, J. J. A. and Hsu, C. C., *J. Macromol. Sci. Rev. Macromol. Chem. Phys.*, **C33**, 103 (1993).
Fairbrother, D. H., Roberts, J. G. and Somorjai, G. A., *Surf. Sci.*, **399**, 109 (1998).
Fairbrother, D. H., Roberts, J. G., Rizzi, S. and Somorjai, G. A., *Langmuir*, **13**, 2090 (1997).
Fink, G., Mülhaupt, R. and Brintziger, H. H. "Ziegler Catalysis," (eds).

Springer-Verlag, Heidelberg (1994).
For example, ref. 3, p. 295.
Fuhrmann, H. and Herrmann, W., *Macromol. Chem. Phys.*, **195**, 3509 (1994).
Gracias, D. H. and Somorjai, G. A., *Macromolecules*, **31**, 1269 (1998).
Gross, T., Lippitz, A., Unger, W. E. S., Friedrich, J. and Woll, C., *Polymer*, **35**, 5901 (1994).
Guerra, G., Pucciariello, R., Villani, V. and Corradini, P., *Polym. Commun.*, **28**, 100 (1987).
Gunter, P. L. J., Niemantsverdriet, J. W., Ribeiro, F. H. and Somorjai, G. A., *Catal. Rev.-Sci. and Eng.*, **39**, 77 (1997).
Gutman, J. Y. and Guillet, J. E., *Macromolecules*, **3**, 470 (1970).
Guttman, J. Y. and Guillet, J. E., *Macromolecules*, **1**, 461 (1968).
Hamba, M., Han-Adebekun, G. C. and Ray, W. H., *J. Polym. Sci. Polym. Chem.*, **35**, 2075 (1997).
Hasebe, K., Mori, H. and Terano, M., *J. Mol. Catal. A*, **124**, L1 (1997).
Hayashi, T., Inoue, Y., Chujo, R. and Doi, Y., *Polymer*, **30**, 1714 (1989).
Kakugo, M., Sadatoshi, H., Sakai, J. and Yokoyama, M., *Macromolecules*, **22**, 22 (1989).
Kakugo, M., Sadatoshi, H., Yokoyama, M. and Kojima, K., *Macromolecules*, **22**, 547 (1989).
Kashiwa, N. and Yoshitake, J., *Makromol. Chem.*, **185**, 1133 (1984).
Keii, T., Suzuki, E., Tamura, M., Murata, M. and Doi, Y., *Makromol. Chem.*, **183**, 2285 (1982).
Keii, T., "Kinetics of Ziegler-Natta Polymerization," Kodanasha, Tokyo (1972).
Kim, S. H. and Somorjai, G. A. *Appl. Surf. Sci.*, **161**, 333 (2000a).
Kim, S. H. and Somorjai, G. A., *Catal. Lett.*, **66**, 5 (2000c).
Kim, S. H. and Somorjai, G. A., *J. Phys. Chem. B* (in press).
Kim, S. H. and Somorjai, G. A., *J. Phys. Chem. B*, **104**, 5519 (2000b).
Kim, S. H. and Somorjai, G. A., *J. Phys. Chem. B*, **105**, 3922 (2001).
Kim, S. H. and Somorjai, G. A., *Surf. Interface Anal.*, **31**, 401 (2001).
Kim, S. H., Magni, E. and Somorjai, G. A., *Stud. Surf. Sci. Catal.*, **130**, 3861 (2000a).
Kim, S. H., Tewell, C. R. and Somorjai, G. A. *Langmuir*, **16**, 9414 (2001).
Kim, S. H., Vurens, G. and Somorjai, G. A. *J. Catal.*, **193**, 171 (2000b).
Kissin, Y. V., "Isospecific Polymerization of Olefins with Heterogeneous Ziegler-Natta Catalysts," Springer, New York (1985).
Kohara, K., Shinogama, M., Doi, Y. and Keii, T., *Makromol. Chem.*, **180**, 2139 (1979).
Lin, J. S. and Catlow, C. R. A., *J. Mater. Chem.*, **3**, 1217 (1993).
Lorenzo, V., Perena, J. M. and Fatou, J. G., *J. Mater. Sci. Lett.*, **8**, 1455 (1989).
Magni, E. and Somorjai, G. A., *Appl. Surf. Sci.*, **89**, 187 (1995a).
Magni, E. and Somorjai, G. A., *Catal. Lett.*, **35**, 205 (1995c).
Magni, E. and Somorjai, G. A., *J. Phys. Chem. B*, **102**, 8788 (1998).
Magni, E. and Somorjai, G. A., *J. Phys. Chem.*, **100**, 14786 (1996b).
Magni, E. and Somorjai, G. A., *Surf. Sci.*, **341**, L1078 (1995b).
Magni, E. and Somorjai, G. A., *Surf. Sci.*, **345**, 1 (1996a).
Magni, E. and Somorjai, G. A., *Surf. Sci.*, **377**, 824 (1997).
Mckenna, T. F., Dupuy, J. and Spitz, R., *J. Appl. Polym. Sci.*, **57**, 371 (1995).
Noristi, L., Marchetti, E., Baruzzi, G. and Sgarzi P., *J. Polym. Sci. A: Polym. Chem.*, **32**, 3047 (1994).
Ogawa, T., *J. Appl. Polym. Sci.*, **44**, 1869 (1992).
Paukkeri, R., Vaananen, T. and Lehtinen, A., *Polymer*, **34**, 4075 (1993).
Petts, R. W. and Waugh, K. C., *Polymer*, **23**, 897 (1982).
Puhakka, E., Pakkanen, T. T. and Pakkanen, T. A., *J. Mol. Catal. A*, **120**, 143 (1997).
Puhakka, E., Pakkanen, T. T. and Pakkanen, T. A., *Surf. Sci.*, **334**, 289 (1995).
Rainer, D. R. and Goodman, D. W., *J. Mol. Catal. A*, **131**, 259 (1998).
Roberts, J. G., Gierer, M., Fairbrother, D. H., van Hove, M. A. and Somorjai, G. A., *Surf. Sci.*, **399**, 123 (1998).
Rodriguez, L. A. M., Van Looy, H. M. and Gabant, J. A., *J. Polym. Sci. A-1*, **4**, 1905 (1966).
Rodriguez, L. A. M., Van Looy, H. M. and Gabant, J. A., *J. Polym. Sci. A-1*, **4**, 1971 (1966).
Santa Maria, L. C., Coutinho, F. M. and Bruno, J. C., *Eur. Polym. J.*, **29**, 1319 (1993).
Shariati, A., Hsu, C. C. and Bacon, D. W., *Polym. Reac. Eng.*, **7**, 97 (1999).
Shen, Y. R., *Ann. Rev. Phys. Chem.*, **40**, 327 (1989).
Shiga, A., Kawamura-Kuribayashi, H. and Sasaki, T., *J. Mol. Catal.*, **87**, 243 (1994).
Shiga, A., Kawamura-Kuribayashi, H. and Sasaki, T., *J. Mol. Catal.*, **98**, 15 (1995).
Soga, K. and Shiono, T., *Prog. Polym. Sci.*, **22**, 1503 (1997).
Soga, K., Chen, S. I. and Ohnishi, R., *Polymer Bull.*, **4**, 157 (1981a).
Soga, K., Sano, T. and Ohnishi, R., *Polymer Bull.*, **8**, 473 (1981b).
Somorjai, G. A., "Introduction to Surface Chemistry and Catalysis," Wiley, New York (1994).
Spitz, R., Lacombe, J. L. and Guyot, A., *J. Polym. Sci., Polym. Chem. Ed.*, **22**, 2625 (1984).
Stair, P. C. and Li, C., *J. Vac. Sci. Tech. A*, **15**, 1679 (1997).
Su, X., Cremer, P. S., Shen, Y. R. and Somorjai, G. A., *J. Am. Chem. Soc.*, **119**, 3994 (1997).
Su, X., Cremer, P. S., Shen, Y. R. and Somorjai, G. A., *Phys. Rev. Lett.*, **77**, 3858 (1996).
Tewell, C. R., Malizia, F., Ager, J. W. and Somorjai, G. A., *J. Phys. Chem. B* (submitted).
Valle, G., Baruzzi, G., Paganetto, G., Depaoli, G., Zannetti, R. and Marigo, A., *Inorg. Chim. Acta.*, **156**, 157 (1989).
Venditto, V., Guerra, G. and Corradini, P., *Eur. Polym. J.*, **27**, 45 (1991).
Woodruff, D. P. and Delchar, T. A., "Modern Techniques of Surface Science," Cambridge University Press, Cambridge (1994).
Xie, T., McAuley, K. B., Hsu, J. C. C. and Bacon, D. W., *Ind. Eng. Chem. Res.*, **33**, 449 (1994).
Zhang, D., Shen, Y. R. and Somorjai, G. A., *Chem. Phys. Lett.*, **281**, 394 (1997).
Zuiker, C. D., Gruen, D. M. and Krauss, A. R., *MRS Bull.*, **20**(5), 29 (1995).